# Propagation dynamics of individual shear bands during inhomogeneous flow in a Zr-based bulk metallic glass

R. Maaß, D. Klaumünzer, J.F. Löffler *

Laboratory of Metal Physics and Technology, Department of Materials, ETH Zurich, Wolfgang-Pauli-Strasse 10, 8093 Zurich, Switzerland

## Abstract

In this study, shear-band propagation during serrated and non-serrated flow of a bulk metallic $Zr_{52.2}Ti_5Cu_{17.9}Ni_{14.6}Al_{10}$ (Vit105) glass was investigated. It was found that individual flow serrations can be directly linked to the activation of a single shear band. Rather than reflecting an intrinsic property of the metallic glass, displacement jump magnitudes are shown to be dependent on external factors such as sample and machine compliances. The need to correct experimentally determined displacement jump magnitudes is highlighted, and a solution is presented taking into account the sample–machine assembly. Using these corrected values, an Arrhenius behavior is established on the part of the shear-band propagation velocity of over four orders of magnitude, ranging from $10^{-2}$ to $10^{-6}$ m s$^{-1}$ for temperatures between 50 °C and −100 °C. It is shown that the transition from serrated to non-serrated flow can be directly linked to the shear-band propagation velocity, such that the transition occurs at the temperature for which the shear-band velocity equals that of the cross-head velocity applied during the test. Non-serrated flow hence corresponds to a state in which a shear band can be continuously driven at a defined rate in the absence of shear-band arrest.

## 1. Introduction

The mechanical properties of bulk metallic glasses have been studied extensively in recent years [1–4], owing to both the fundamental scientific interest they have generated and their potential for use in engineering applications. It is well established that, at low homologous temperatures $(T/T_g < 0.8)$ metallic glasses typically deform by flow localization such that all the plastic strain sustained by the sample is confined to narrow shear bands. Flow localization is the consequence of a softening mechanism, which has been attributed, for example, to shear-band heating or stress-induced shear-band dilatation, and can more generally be summarized as being of thermal or mechanical origin [5–8]. It is generally believed that this softening mechanism is an autocatalytic process

[9], generating rapid, brittle failure of metallic glasses in tension, as well as in many, but not all, alloys under compression, thus limiting their use in applications. Some metallic glasses, however, undergo shear banding in a stable manner without catastrophic failure and autocatalytic softening. Such behavior can be observed during uniaxial compression and is reflected in a series of discrete, rapid shear events, as is apparent from stress drops (serrations) [10]. This is similar to pop-ins appearing during nanoindentation [11,12], with the important difference that stable deformation is intrinsically imparted by the indentation method's boundary conditions. In both cases, each discrete shear event corresponds to a single cycle of shear band (re)initiation, propagation and arrest. While the resulting serrated flow curves in compression tests suggest an apparently ductile behavior on the part of the glass, and values of the overall ductility are commonly stated in the literature (e.g., Ref. [13]), homogeneous macroscopic plasticity within these metallic glasses is generally

* Corresponding author.
  E-mail address: joerg.loeffler@mat.ethz.ch (J.F. Löffler).

not observed, because shear banding and flow localization prevails.

The origin of stable shear-band propagation and serrated flow remains elusive, but attempts have been made to attribute these effects to intrinsic and extrinsic materials properties [2] as well as to experimental factors [14]. One of the most prominent examples of intrinsic properties influencing ductility, here understood as stable shear banding, was shown by Lewandowski et al. to be associated with a critical Poisson's ratio of 0.32, below which a metallic glass was expected to behave in a brittle manner [15]. In addition, the free volume content has been found to influence the ductility of metallic glasses with structural annealing [16] or aging [17], leading to embrittlement due to a reduction in free volume, and structural disordering due to ion irradiation showing the exact opposite effect [18]. Besides these intrinsic properties of monolithic metallic glasses, numerous studies have demonstrated that the ductility of metallic glasses can be improved extrinsically by introducing an additional phase to form bulk metallic glass composites [19,20]. In such cases, secondary phases are believed to have effects on both shear-band nucleation and propagation during serrated flow, yielding a higher shear-band density; that is, a higher plastic strain is distributed over a larger sample volume. In addition to these intrinsic and extrinsic material properties, enhanced apparent plasticity may also be a consequence of geometrical constraints during mechanical testing [14,21]. For instance, after a carefully conducted series of compression tests, Wu et al. [14] reported that any deviation from a perfect coaxial alignment of the sample with respect to the compression axis results in a larger apparent plasticity.

Despite the ongoing debate regarding its origin, serrated inhomogeneous plastic flow has been studied extensively [22–30]. In time-resolved compression tests, it was recently shown that the duration as well as the shear-band velocity of individual shear events can be determined [25,26]. The interest in measuring the time scales associated with shear banding stems mainly from the desire to identify the origin of flow softening and attribute it to a mechanical or thermal effect. In fact, by evaluating flow serrations as a function of temperature, it was shown by the authors of the present study that shear-band propagation follows a thermally activated mechanism with an associated activation energy of $\sim$0.3 eV [29]. The results also reveal that shear banding occurs in a highly controlled rather than a catastrophic manner in the case of serrated flow.

This paper shows that the disappearance of flow serrations on increasing the externally applied strain rate or lowering the temperature [22,27] can be directly linked to the dynamics of shear-band propagation. It also shows that the macroscopic shear-band velocities measured can be attributed to the operation of a single shear band and that the temperature dependence observed is not dominated by changes in the shear-band nucleation rate. In addition, it is demonstrated that the total shear offset generated during a single serration is composed of machine and sample contributions, of which only the machine contribution is reflected in the recorded displacement jump. This finding also explains the discrepancy between total shear offset and strain jump magnitude, as obtained from strain gauge measurements [31].

## 2. Experimental details

Uniaxial compression tests were conducted using cylindrical samples of glassy $Zr_{52.2}Ti_5Cu_{17.9}Ni_{14.6}Al_{10}$ (Vit105) 3 mm in diameter, which were prepared by suction casting in an arc-melter. All samples were lapped on the end surfaces with a 3-μm SiC suspension to ensure the best coaxial alignment possible. Compression tests were conducted at 50–100 °C at nominal cross-head velocities between 0.01 and 3 mm s$^{-1}$, corresponding to strain rates of $10^{-5}$ s$^{-1}$ and $10^{-2}$ s$^{-1}$, respectively. An extensometer bridging the upper and lower compression platens was used to record the displacement, and a piezoelectric load cell was employed to measure the load during the tests. Data was acquired at rates of 10 kHz using an AD-converter with a moving average filter over eight consecutive points, allowing for a time resolution of 300 μs for individual stress drops. Further details regarding the setup can be found in Ref. [29]. In addition to the as-cast samples, rectangular samples were prepared from the same rods produced in the arc-melter. These samples were polished on all four vertical sides with a final polishing step consisting of a 1/4-μm diamond suspension. Successive, interrupted compression tests and scanning electron microscopy (SEM) (Hitachi SU70) investigations were conducted to follow the shear-band morphology between individual serrations.

## 3. Results and discussion

### 3.1. Shear-band density and offsets during serrated flow

Despite the numerous studies concerning in situ imaging of shear-band dynamics [31–33] or, more precisely, correlating shear operations with stress drops [24,34–36], in metallic glasses, no common agreement has been reached on whether a macroscopic shear event, as reflected in flow serrations, can be attributed to the operation of a single shear band or multiple shear bands. In addition, changes in the characteristics of serrated flow have been reported to coincide with changes in shear-band density as a function of temperature or strain rate [34,37]. Models focusing on the nucleation kinetics of shear bands for individual shear events have been proposed to explain these effects [1,38,39].

In quantifying the dynamics of individual shear events by calculating shear-band velocities, it is commonly assumed that shear occurs within a single band only [25,26,29]. In order to verify this assumption, i.e., whether a macroscopic load drop and strain jump can be associated with shear on a single shear plane only, the shear-band morphology of a carefully polished sample was analyzed

before and after a single load drop. Owing to uncertainties with respect to resolving small load drops, a reference state was set within a preliminary compression cycle in which the test was stopped after the first four macroscopic serrations were observed. SEM analysis revealed that two major shear bands (labeled SB1 and SB2 in Fig. 1a) had formed after attaining the reference state. The shear offset of the reference state could be determined as equal to 1.95 μm for shear band SB1 (Fig. 1b). On reloading the sample, the test was immediately interrupted after the first serration was observed. From the recorded load and displacement data, the magnitude of the corresponding uniaxial displacement burst and load drop (Fig. 1d) could be determined as 2.75 μm and 400 N, respectively. Analysis of the evolution of the shear-band morphology revealed that no additional shear band had formed, but that the shear offset of SB1 had grown to 6.93 μm, as displayed in Fig. 1c. Hence, in the present case a single load drop directly corresponds to the activation of a single shear band.

The measured uniaxial displacement burst can be related to the actual shear offset by introducing the following correction. The response of the machine–sample assembly during serrated flow can be visualized by a simple model as described in Refs. [22] and [40] and reproduced in the inset of Fig 2a. The model essentially consists of three parts: two springs to model the elastic response of the sample as well as the machine, and a shear band accommodating plastic deformation in the sample. It is understood that the process of shear-band operation is intermittent, i.e., the band follows repeated cycles of initiation, propagation and arrest as a function of loading history (see Fig. 2a). On progressive loading between $t_0$ and $t_i$, elastic displacement is
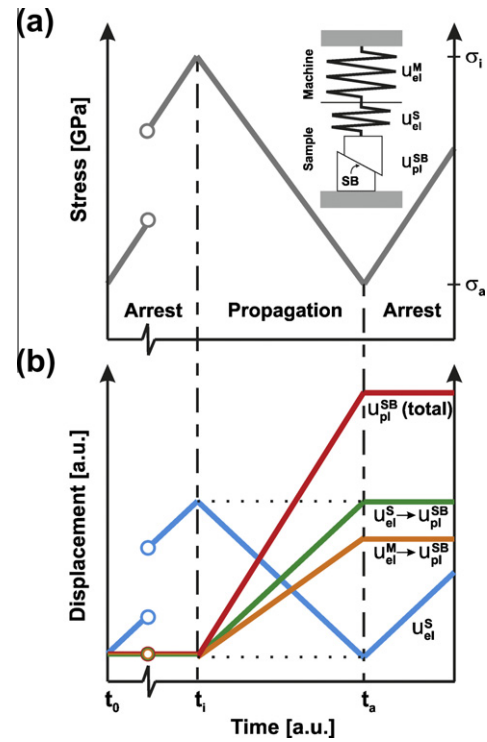


Fig. 2. Schematics showing (a) the stress and (b) the displacement evolution during one flow serration cycle. The inset in (a) represents the elastic and plastic properties of the sample–machine assembly. In (b) it is seen that at $t_a$ (the end of the load drop) both the elastic displacement from the sample, $u_{el}^S \rightarrow u_{pl}^{SB}$, and the elastic recovery of the machine, $u_{el}^M \rightarrow u_{pl}^{SB}$, add to the total plastic displacement $u_{pl}^{SB}$(total). Based on the close-to-identical compliances of both the sample and the machine, their elastic displacements as a function of time are assumed to be identical (see also Section 3.2).
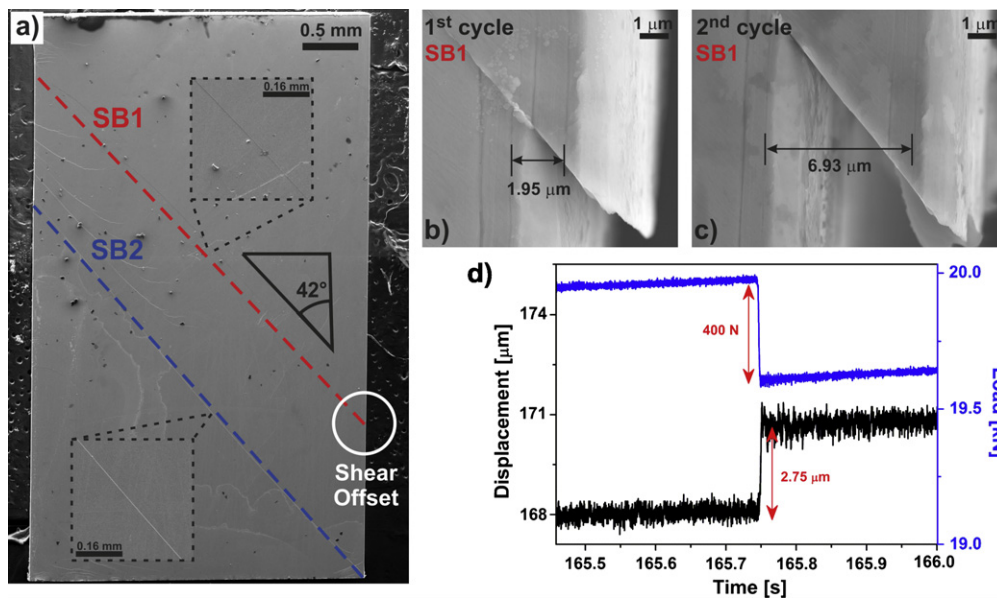


Fig. 1. (a) Rectangular polished sample prior to the second loading cycle: two fully transecting shear bands can be distinguished (SB1 and SB2), of which the shear offset of SB1 was determined as 1.95 μm (see (b)). The two insets in (a) highlight short parts of both SB1 and SB2. (b) Shear offset of SB1 before reloading the sample to generate one additional load drop. (c) Shear offset after the second loading cycle consisting of one load drop; the shear offset of SB1 increased to 6.93 μm. (d) Corresponding load drop and displacement jump of the individual serration occurring during the second loading cycle.

accumulated within both sample and machine, while the shear band is at rest. At a critical peak load ($\sigma_i$), a shear band is initiated. The shear band effectively corresponds to a thin layer of softened material allowing plastic flow to be accommodated at decreasing stress. Hence, the load drops during the propagation stage until a critical lower limit is reached, at which the shear-band arrests ($\sigma_a$). The plastic displacement $u_{pl}^{SB}$ imparted into the sample during this discrete shear event can be deduced as follows. It is important to bear in mind that only the material volume contained in the shear band undergoes plastic deformation. Owing to the low shear-band thickness ($\sim$20 nm), this is only a small fraction of the total sample volume. The remaining glass is still allowed to relax elastically on changes in load. It is clear that the elastic displacements recovered by the sample $u_{el}^S$ and the machine $u_{el}^M$ are proportional to the load drop magnitude $\Delta F$ as well as the respective compliances $C_S$ and $C_M$. Assuming that the total displacement in the system remains constant, the sum of elastic strain recovered by the sample and machine is equal to the plastic strain imparted into the sample $u_{pl}^{SB}$:

$$u_{pl}^{SB} = u_{el}^S + u_{el}^M = \Delta F(C_M + C_S) \qquad (1)$$

Fig. 2b represents a schematic timeline of the evolution of strain within the sample–machine assembly as discussed above. On increasing the load (reloading), elastic strain is imparted into both sample and machine which is then converted into plastic strain as the load drops during shear-band propagation. The amount of elastic strain recovered in the entire system is directly balanced by the magnitude of plastic strain imparted solely into the sample (see Eq. (1)).

The above analysis of the partitioning of strain in the machine–sample assembly during shear events reveals direct implications for the experimental procedure of measuring strain burst magnitudes. Typically, an extensometer is used to monitor sample length during the compression test. Considering that the strain burst magnitude is composed of two contributions originating from the elastic response of the machine and the sample, it is clear that only the machine contribution can be detected experimentally. This is because a direct conversion of elastic to plastic strain in the sample does not result in any immediate net change in length. In other words, taking strain burst magnitudes directly from the measured displacement signal yields an underestimate by a term corresponding to the sample contribution $u_{el}^S$. Hence, this term needs to be added to the measured value in order to determine the correct strain burst magnitude, as expressed by Eq. (1).

Eq. (1) can in fact be verified geometrically from a plot of load vs recorded uniaxial displacement by determining the total uniaxial displacement over both the loading and unloading segments for an event of given magnitude $\Delta F$ (see inset to Fig. 3). Plotting the measured values of $\Delta u_{total}$ against those determined from Eq. (1) for a larger set of serrations yields good agreement, as shown in Fig. 3.
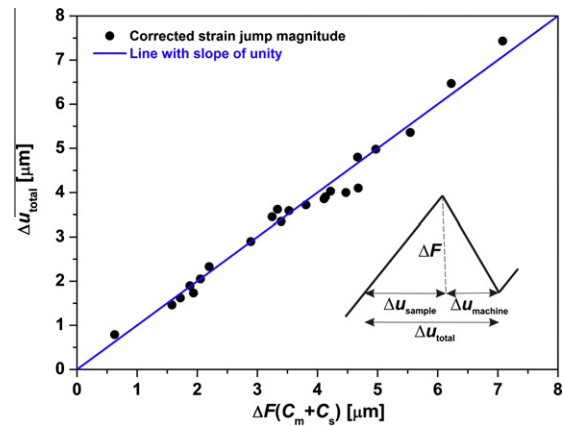


Fig. 3. Total strain per stress drop and previous elastic loading portion (see inset) as a function of the calculated total displacement by summing the sample and machine contributions according to Eq. (1).

The model can now be used to correct the measured displacement burst generated in the second compression cycle of the sample presented in Fig. 1. For a load drop of 400 N and an experimentally determined sample compliance of 7.3 nm N$^{-1}$, the uniaxial elastic strain recovered by the sample amounts to 2.92 μm. Adding this value to the recorded strain jump (2.75 μm), i.e., the uniaxial strain recovered by the machine, yields a total uniaxial displacement burst of 5.67 μm. For a shear band inclined at 42° relative to the compression axis (as for shear band SB 1), this equates to a total (horizontal) shear offset of 5.10 μm. This value is in good agreement with the increase in shear-offset size by 4.98 μm on reloading the sample, as determined from the corresponding SEM micrographs (Fig. 1b and c). Thus, the above results verify the initial assumption and confirm the view proposed in Refs. [24] and [31], i.e., the entire macroscopic plastic strain formed during discrete shear events is due to the operation of a single shear band. By evaluating the parameters for the shear-band velocity from the individual serrations, the dynamics of single shear bands can therefore be quantified rather than those of an assembly of collectively acting bands. It is also worth noting that an evaluation of shear-band velocities from displacement jumps underestimates the shear-band velocity by a factor which depends on the sample compliance. In this respect, shear displacement jump magnitudes do not reflect an intrinsic property of the glass, but are influenced by external factors, i.e., sample geometry and machine characteristics such as compliance. In this context, it is interesting to remark that recent work has addressed the issue of shear-band stability as a function of sample diameter and machine stiffness. Samples were found to embrittle as a function of increasing sample diameter or decreasing machine stiffness [40].

### 3.2. Regimes of inhomogeneous flow

A temperature and strain-rate dependent transition from intermittent, serrated flow to continuous, non-serrated

flow has been widely studied in the literature for different alloy systems [22,27,39]. This change in deformation mode has been attributed to changes in the nucleation kinetics and density of shear bands [39] as well as to a diffusional relaxation mechanism of free volume [27]. In the following, it will be shown that, by determining shear-band velocities at this transition, the mode of inhomogeneous flow can be directly related to the dynamics of shear-band propagation.

Fig. 4a shows the uniaxial displacement signal of two compression tests conducted at a common temperature of $-30\,°C$ and different cross-head velocities of $v_{XH1} = 0.005\,\text{mm s}^{-1}$ and $v_{XH2} = 0.05\,\text{mm s}^{-1}$. While discrete displacement bursts are observed for the lower strain rate, a continuous signal is present at the higher rate. Thus, by increasing the strain rate of the test, a transition from serrated to non-serrated flow can be initiated. Fig. 3b shows the corresponding shear-band velocity calculated from the derivative of the displacement signal in Fig. 3a with respect to time $t$, and by resolving the uniaxial displacement for a shear plane oriented at $45\,°C$ relative to the load axis, i.e.,

$$v_{SB} = \sqrt{2}\frac{\Delta u}{\Delta t} \tag{2}$$

where $\Delta u$ is the total change in displacement. In the case of serrated flow, this displacement corresponds to the magnitude of discrete strain jumps and needs to be corrected in order to account for the sample contribution as given by Eq. (1). Since for the specific sample geometry used the compliances of the machine $C_M$ (8.0 nm N$^{-1}$) and the sample $C_S$ (7.3 nm N$^{-1}$) are very close, it is reasonable to approximate $v_{SB}$ by $= 2\sqrt{2}\Delta u'/\Delta t$, where $\Delta u'$ is the measured displacement burst.

In agreement with earlier work [29], it can be seen from Fig. 4b that, for discrete shear events, the shear band attains velocities close to 0.07–0.08 mm s$^{-1}$ at a testing temperature of $-30\,°C$. This is much greater than the applied cross-head velocity of 0.005 mm s$^{-1}$ ($v_{XH1}$). In the absence of discrete shear events (load drops/strain jumps), at a cross-head velocity of 0.05 mm s$^{-1}$ ($v_{XH2}$), the associated shear-band velocity simply corresponds to the velocity applied in the test, which is comparable or exceeds the shear-band velocity determined at the same temperature under conditions of serrated flow. In the specific case of non-serrated flow shown in Fig. 4b, the shear-band velocity indeed reproduces the applied cross-head velocity resolved for a shear plane oriented at 45° (0.07–0.08 mm s$^{-1}$).

The above result can be generalized by analyzing the transition from serrated to non-serrated flow over a wide range of temperatures and strain rates. Fig. 5a shows a plot of shear-band velocity as a function of inverse temperature for serrated and non-serrated flow at different strain rates, complementing data presented in previous work [29]. All data presented in Fig. 5a were derived in a regime of constant flow stress, i.e., within a stress plateau. Note that the shear-band velocities for serrated flow in Fig. 5a are greater than in Ref. [29] by approximately a factor of two, because here the corrected $\Delta u_{total}$ (including the sample contribution) was used. The shear-band velocities determined in the serrated flow regime follow the linear trend of a thermally activated mechanism, providing evidence that shear banding is not an autocatalytic catastrophic, but a controlled process. The activation energy for shear-band propagation was estimated to be 0.32 eV by fitting the data in Fig. 5a. This linear trend is conserved independent of applied strain rate, allowing shear bands as slow as $10^{-6}$ m s$^{-1}$ to be captured. This corresponds to shear event duration as long as 2 s, much higher than any other value stated in the literature [25,26]. In contrast, the shear-band velocities associated with non-serrated flow simply reproduce the respective velocity applied in the test independent of temperature. This is apparent from the blue-square data points lying on the dashed horizontal lines of the resolved
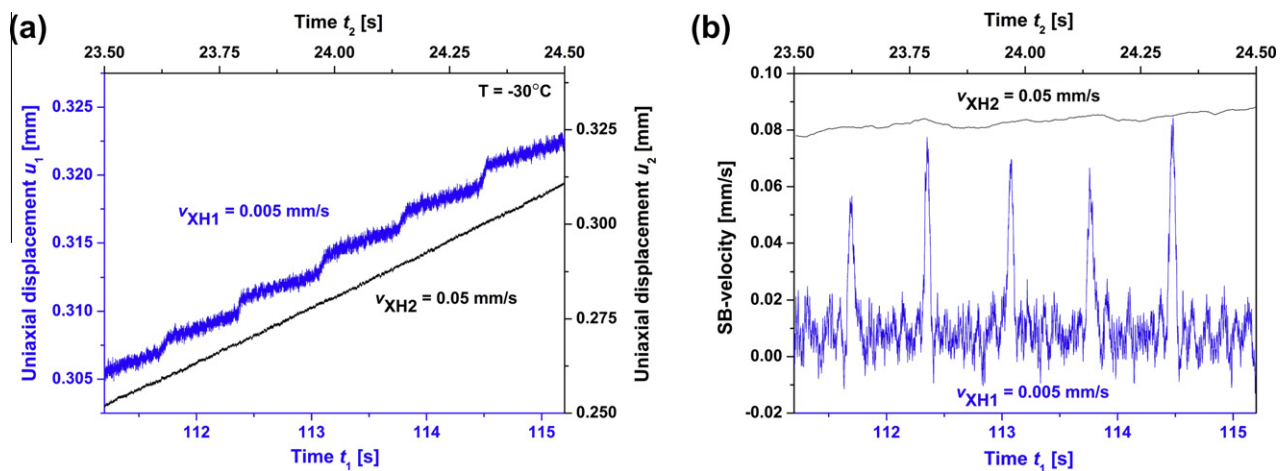


Fig. 4. (a) Uniaxial displacement signal for two compression tests conducted at $-30\,°C$ with different cross-head velocities $v_{XH}$. The slow cross-head velocity test features distinct displacement jumps, whereas the higher cross-head velocity test corresponds to a continuous displacement increase. (b) Shear-band velocity for both signals depicted in (a): clear velocity spikes are seen in the case of serrated flow ($v_{XH1} = 0.005$ mm s$^{-1}$), and a smooth shear velocity that amounts to the applied cross-head velocity is seen in the non-serrated flow regime ($v_{XH2} = 0.05$ mm s$^{-1}$, in axial measures).
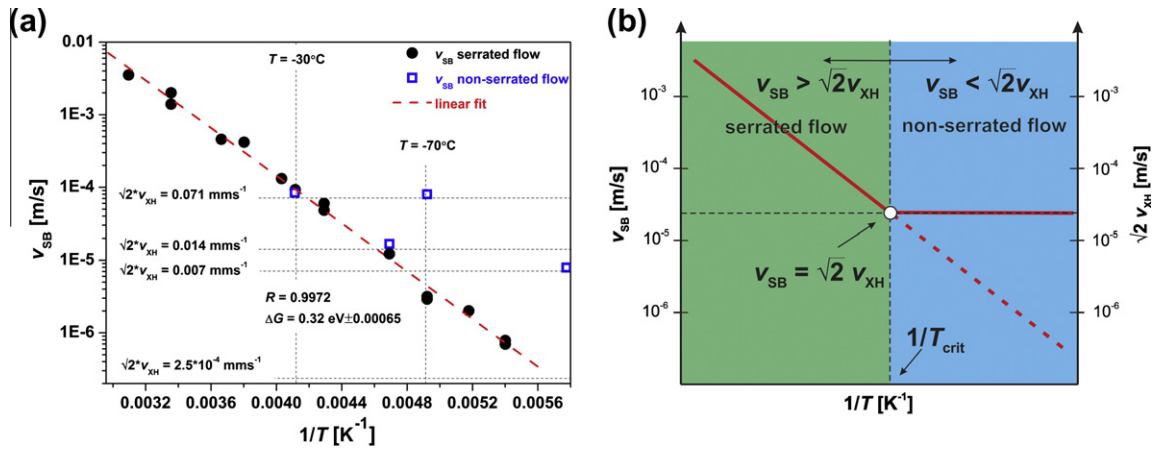
Fig. 5. (a) Shear-band velocity for serrated flow (round symbols) and non-serrated flow (square symbols) recorded at different strain rates. From the Arrhenius behavior of serrated flow an activation energy for thermally activated shear-band propagation is estimated to be 0.32 eV. The horizontal dashed lines indicate the resolved applied cross-head velocity and the vertical lines represent constant testing temperatures. (b) Schematic graph deduced from the data presented in (a). Below a critical temperature $T_{crit}$, at which the shear-band velocity equals $\sqrt{2} \times v_{XH}$, flow becomes non-serrated because $\sqrt{2} \times v_{XH}$ is larger than the shear-band velocity $v_{SB}$.

applied cross-head velocities seen in Fig. 5a. The shear-band velocities of both serrated and non-serrated flow discussed in Fig. 4 can be seen to fall very closely together in Fig. 5a. During shear-band propagation, the shear band in the serrated regime attains velocities that are close to (Fig. 4b) or larger than the applied cross-head velocity, whereas in the non-serrated regime the shear band is driven and limited by the applied cross-head velocity.

The critical temperature of the transition from serrated to non-serrated flow at a given strain rate hence corresponds to the temperature at which the shear-band velocity (round symbols in Fig. 5a) equals the applied cross-head velocity in the test.

At a constant temperature, as indicated by vertical dashed lines in Fig. 5a, serrated flow is only observed when the chosen $v_{XH}$ lies below the intersection of the constant temperature line and the trend line of the thermally activated shear-band velocity. It can therefore be concluded that non-serrated flow is the consequence of overwhelming the shear-band velocity with the cross-head velocity, driving shear bands at a defined rate. Based on this result, it is now possible to establish a schematic graph which contains the testing temperature $T$, the resolved applied cross-head velocity and the shear-band velocity, as depicted in Fig. 5b. For a given temperature, a corresponding shear-band velocity $v_{SB}$ exists, which needs to be greater than the resolved applied cross-head velocity $\sqrt{2} \times v_{XH}$ in order to observe serrated flow.

It is known from the literature that the shear-band velocity increases in the serrated regime when approaching failure [22,26], because of accumulated structural damage in the activated shear bands. Therefore, it is expected that a transition from initially non-serrated to serrated flow can occur during a single test near the crossing at which the shear-band velocity suddenly exceeds the test velocity. This effect is likely to be observed in tests conducted close to the critical temperatures and strain rates. An example is given in Fig. 6: as structural damage proceeds, the shear-band velocity increases and serrated flow sets in owing to the shear-band velocity exceeding the applied cross-head velocity.

In the above analysis for non-serrated flow, it has so far been assumed that shear occurs within a single band only, as has been shown to be the case for serrated flow in Section 3.1. This view, however, contrasts with the fact that the origin of non-serrated flow has been attributed to a nucleation-limited mechanism, i.e., non-serrated flow was proposed to occur as a consequence of a single shear band not being able to accommodate the imposed strain rate during its nucleation stage [1]. Some studies support this model and report an increasing shear-band density with
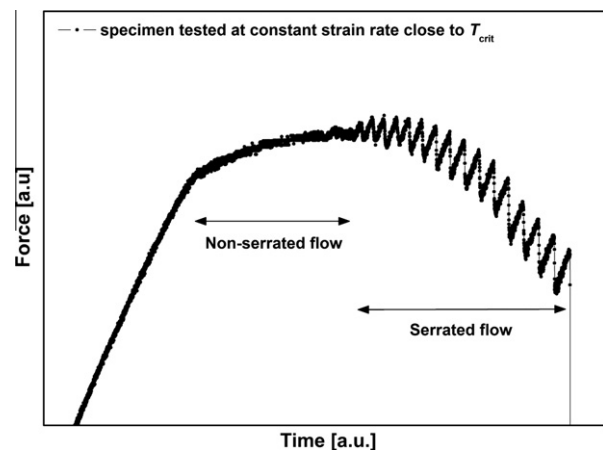


Fig. 6. Compression test conducted with initial conditions set for non-serrated flow, showing a transition to serrated flow after some time. The transition occurs when the shear-band velocity increases owing to accumulated structural damage. In consequence, the shear-band velocity eventually exceeds the applied cross-head velocity.

decreasing temperature and increasing strain rate [34,41,42], while another details the exact opposite effect [37]. Via a carefully conducted SEM analysis of a partially deformed specimen tested to a plastic strain of 2.8% at −60 °C in the non-serrated regime, it can now be shown that shear was fully accommodated by a single band (see Fig. 7a). It must be emphasized, however, that such a clean shear-band morphology requires compression testing to be performed at the highest level of care. This applies particularly to sample alignment and surface quality, to prevent the effects of geometrical constraints and surface stress concentrations which generate diffuse shear banding and the nucleation of several major shear bands at the end surfaces of the sample [14,21]. In contrast to Fig. 7a, an example of a compression test carried out on a misaligned sample of poor surface quality is depicted in Fig. 7b, showing the presence of multiple shear bands. While it is not clear whether all samples representing the non-serrated flow regime in Fig 5a represent cases of single or multiple shear bands, Fig. 7a confirms that non-serrated flow can be observed to reflect the behavior of a single shear band only. Thus the crossover in flow behavior is independent of shear-band density.

The above analysis shows that non-serrated flow is the consequence of overwhelming the shear-band velocity with the applied test velocity, driving a single shear band continuously at a defined rate in the absence of shear-band arrest. The transition from serrated to non-serrated flow can hence be directly attributed to the dynamics of single shear-band propagation.

The occurrence of non-serrated flow mediated by a single shear band is an interesting observation, particularly with respect to the shear-band nucleation dynamics model proposed by Schuh and co-workers [39,43]. Their model is derived from indentation testing, during which it was observed that flow serrations became close to absent with increasing strain rates and decreasing temperature. In a related deformation map, the region of high strain rates was termed "homogeneous II", in which flow tended to homogenize in both time and space with increasing strain rate or decreasing temperature. The underlying idea of the shear-band nucleation kinetics model is that collectively acting shear-transformation zones (STZs) represent a shear-band nucleation limiting process via the formation of a shear-band nucleus. Creating a shear-band nucleus, i.e., a collection of STZs, obeys a specific natural frequency. Schuh et al. described the transition from "inhomogeneous" (here understood as serrated) to "homogeneous II" flow in their nanoindentation experiments using this athermal frequency, which was successfully applied to fit the boundary between "inhomogeneous" and "homogeneous II"-type flow. Based on this, it was concluded that a kinetic limitation exists when strain-rate partitioning from the bulk into a shear band is not efficient enough, leading to a higher shear-band nucleation rate and eventually to homogenization of flow to accommodate the imposed strain. Several experimental reports under loading conditions different from indentation have shown a higher shear-band density with increasing strain rate [44] or decreasing temperature [45], thus supporting the shear-band nucleation dynamics model. Therefore, it has become customary to also explain the typically observed increasing relative shear-band density in the non-serrated regime with decreasing temperature by an increased shear-band nucleation rate. The above demonstration of imparting the applied strain rate entirely into a single shear band challenges the use of this model in the regime of non-serrated flow during compression testing. In fact, the results presented here show that the applied strain rate can be imposed onto a single shear-band instability without the requirement of nucleating multiple ones.

A possible explanation for the disagreement of the present results with the shear-band nucleation rate theory is the following. During indentation at higher strain rates (equivalent to lowering the temperature), the indenter tip proceeds fast through the material, thereby suppressing autocatalytic activation of a shear band which, at high enough strain rates, homogenizes deformation. The mechanical conditions during compression testing are, however, very different, and inhomogeneous flow is not affected by limitations in shear-band nucleation kinetics, as supported by the present observations. In fact, during well-conditioned compression testing, the entire specimen volume is under an equivalent stress state, which in combination with a broad distribution of STZ activation energies [46] provides ample possibilities to form a collective STZ/ an embryonic shear band. Once the applied strain rate is accommodated by a flowing shear band, there is no reason to nucleate a new shear band unless stress concentrations arise along the course of the experiment which eventually trigger new shear-band formation in order to accommodate the imposed deformation constraints. In addition, in the work of Schuh et al., shear-band propagation is assumed to be fast, occurring at a small fraction of the
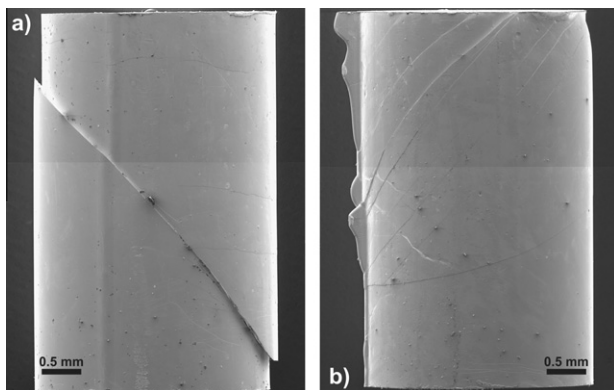


Fig. 7. Very different shear-band morphologies from two samples deformed at the same strain rate under non-serrated conditions, resulting from varying uniaxial alignment perfections in the compression tests: (a) formation of only one single shear band (T = −60 °C); (b) multiple shear banding with predominant shear-band nucleation at the compression anvil interface (T = −50 °C).

Rayleigh velocity (with the Rayleigh velocity being on the order of $10^3$ m s$^{-1}$) [43]. However, for the present alloy, typical room-temperature shear-band velocities take much smaller values of the order of $10^{-3}$ m s$^{-1}$. Hence, within the limits of stable shear banding under uniaxial compression, there is evidence to question whether shear-band nucleation can be taken as the rate-limiting step. It is clear that the transition from serrated to non-serrated flow, as revealed here with compression testing, is not explained by kinetic limitations during the shear-band nucleation stage.

Numerous experimental and theoretical studies have discussed shear-band heating, which occurs during the propagation of a shear band. These studies propose that the temperature rise would be sufficient to reach the glass transition temperature $T_g$, provided that the shear-band propagation (often assumed to be close to the speed of sound) is fast enough [5,47]. Hence it was argued that the time scales of shear-band operation (0.2–1.2 ns) were shorter than those typically associated with thermal conduction (7–167 ns), leaving no time during shear-band propagation for the heat to dissipate into the sample [5]. This argument forms the basis for assuming an instantaneous heat source. Evidence for the validity of this model has been drawn from a correlation between the shear-offset size and the half-width of a zone of molten material of a fusible coating formed around the band at its intersection with the sample surface [47]. However, the results presented here reveal that the duration of discrete shear events during serrated flow can be as long as 2 s on decreasing the temperature to −100 °C. Similarly, for non-serrated flow, strong evidence is provided that continuous sliding occurs over the entire duration of the test, i.e., for time periods of several seconds. In addition, a typical shear offset of 140 μm formed continuously during non-serrated flow before fracture would generate an unreasonably large half-width of a hot zone around the shear band. Thus, modeling the temperature evolution within a shear band using an instantaneous heat source may not be applicable to either serrated or non-serrated flow.

In assessing the influence of shear-band heating, it is therefore necessary to take into account the dynamics of the heat source. Thus, the rate of energy dissipation within the shear band during propagation needs to be balanced against the rate of heat conduction away from the band, as recently shown by Cheng et al. [8]. This simulation work found that significant localized heating coincided with run-away acceleration of shear bands, generating autocatalytic failure while, for stable shear banding, the temperature rise within the band was found to be negligible. It may be inferred that localized heating is not associated with the operation of shear bands *per se*, but is rather a consequence of the dynamics at which the shear process occurs. In other words, provided that sufficient mechanical energy is dissipated sufficiently quickly relative to the rate of heat conduction into the bulk, significant local temperature rises may be observed, generating an autocatalytic acceleration

of the band and runaway failure. However, as is apparent from the dynamics of serrated flow, the shear-band velocities determined in Ref. [29] and extended in this work follow an Arrhenius-type behavior over a narrow temperature range, i.e., shear banding within the limits of stable flow is conceived to occur under thermally equilibrated conditions.

## 4. Conclusions

The above results on the shear-band dynamics in the serrated and non-serrated regimes can be summarized as follows:

1. Successive SEM investigations before and after a single serration reveal that shear during an individual load drop occurs within a single band only.
2. By proposing a simple model for the strain jump magnitude as composed of both a machine and a sample contribution, it is established that the magnitude of a strain jump is not an intrinsic property of the metallic glass, but depends on both the sample geometry and the machine stiffness.
3. Shear-band propagation is a thermally activated process and not catastrophic, as can be established by an Arrhenius plot with a shear-band velocity range of over four orders of magnitude. This behavior is independent of strain rate.
4. The transition from serrated to non-serrated flow corresponds to the point at which the applied machine crosshead velocity overwhelms the shear-band velocity of a single band. A change from serrated to non-serrated flow is directly linked to the dynamics of shear-band propagation and cannot be attributed to kinetic limitations during shear-band nucleation generating an increase in shear-band density. Non-serrated flow is a state in which the shear-band can be continuously driven at a defined rate in the absence of shear-band arrest.
5. The very low shear-band velocities at low temperatures do not favor dramatic temperature rises originating from frictional sliding effects during shear-band propagation.

## References

[1] Schuh CA, Hufnagel TC, Ramamurty U. Acta Mater 2007;55:4067.
[2] Chen M. Ann Rev Mater Res 2008;38:445.
[3] Ashby MF, Greer AL. Scripta Mater. 2006;54:321.

[4] Löffler JF. Intermetallics 2003;11:529.

[5] Lewandowski JJ, Greer AL. Nat Mater 2006;5:15.

[6] Spaepen F. Nat Mater 2006;5:7.

[7] Wright WJ, Schwarz RB, Nix WD. Mater Sci Eng A 2001;229:319–21.

[8] Cheng YQ, Han Z, Li Y, Ma E. Phys Rev B 2009;80:134115.

[9] Argon AS. Acta Metall 1979;27:47.

[10] Chen HS. Scripta Metall 1973;7:931.

[11] Golovin YI, Ivolgin VI, Khonik VA, Kitagawa K, Tyurin AI. Scripta Mater 2001;45:947.

[12] Schuh CA, Nieh TG. Acta Mater 2003;51:87.

[13] Liu YH, Wang G, Wang RJ, Zhao DQ, Pan MX, Wang WH. Science 2007;315:1385.

[14] Wu WF, Li Y, Schuh CA. Phil Mag 2008;88:71.

[15] Lewandowski JJ, Wang WH, Greer AL. Phys Rev Lett 2005;85:77.

[16] Murali P, Ramamurty U. Acta Mater 2005;53:1467.

[17] Castellero A, Uhlenhaut DI, Moser B, Löffler JF. Phil Mag Lett 2007;87:383.

[18] Raghavan R, Boopathy K, Ghisleni R, Pouchon MA, Ramamurty U, Michler J. Scripta Mater 2010;62:462.

[19] Eckert J, Das J, Pauly S, Duhamel C. J Mater Res 2007;22:285.

[20] Siegrist ME, Löffler JF. Scripta Mater 2007;56:1079.

[21] Mondal K, Hono K. Mater Trans 2009;50:152.

[22] Kimura H, Masumoto T. Acta Metall 1983;31:231.

[23] Dalla Torre FH, Dubach A, Schällibaum J, Löffler JF. Acta Mater 2008;56:4635.

[24] Song SX, Bei H, Wadsworth J, Nieh TG. Intermetallics 2008;16:813.

[25] Wright WJ, Samale MW, Hufnagel TC, LeBlanc MM, Florando JN. Acta Mater 2009;57:4639.

[26] Chen HM, Huang JC, Song SX, Nieh TG, Jang JSC. Appl Phys Lett 2009;94:141914.

[27] Dubach A, Dalla Torre FH, Löffler JF. Acta Mater 2009;57:881.

[28] Song SX, Nieh TG. Intermetallics 2009;17:762.

[29] Klaumünzer D, Maass R, Dalla Torre FH, Löffler JF. Appl Phys Lett 2010;96:061901.

[30] Dalla Torre FH, Klaumünzer D, Maass R, Löffler JF. Acta Mater 2010;58:3742.

[31] Song SX, Wang XL, Nieh TG. Scripta Mater 2010;62:847.

[32] Neuhäuser H. Scripta Metall 1978;12:471.

[33] Yang B, Morrison ML, Liaw PK, Buchanan RA, Wang G, Liu CT, et al. Appl Phys Lett 2005;86:141904.

[34] Jiang WH, Liu FX, Liaw PK, Choo H. Appl Phys Lett 2007;90:181903.

[35] Dubach A, Raghavan R, Löffler JF, Michler J, Ramamurty U. Scripta Mater 2009;60:567.

[36] Liu YH, Liu CT, Gali A, Inoue A, Chen MW. Intermetallics 2010;18:1455.

[37] Jiang WH, Jiang F, Liu FX, Choo H, Liaw PK, Qiu KQ. Appl Phys Lett 2006;89:261909.

[38] Li WH, Wei BC, Zhang TH, Xing DM, Zhang LC, Wang YR. Intermetallics 2007;15:706.

[39] Schuh CA, Lund AC, Nieh TG. Acta Mater 2004;52:5879.

[40] Han Z, Wu WF, Li Y, Wei YJ, Gao HJ. Acta Mater 2009;57:1367.

[41] Yoon K-S, Lee M, Fleury E, Lee J-C. Acta Mater 2010;58:5295.

[42] Li H, Tao K, Fan C, Liaw PK, Choo H. Appl Phys Lett 2006;89:041921.

[43] Schuh CA, Argon AS, Nieh TG, Wadsworth J. Phil Mag 2003;83:2585.

[44] Mukai T, Nieh TG, Kawamura Y, Inoue A, Higashi K. Intermetallics 2002;10:1071.

[45] Kawashima A, Zeng Y, Fukuhara M, Kurishita H, Nishiyama N, Miki H. Mater Sci Eng A 2008;498:475.

[46] Rodney D, Schuh C. Phys Rev Lett 2009;102:235503.

[47] Zhang Y, Stelmashenko NA, Barber ZH, Wang WH, Lewandowski JJ, Greer AL. J Mater Res 2007;22:419.